Finite-Difference Simulations of Time Reversed Acoustics in a Layered Earth Model

Rongrong Lu, Nafi Toksoz
Earth Resources Laboratory
Dept. of Earth, Atmospheric and Planetary Sciences
Massachusetts Institute of Technology
Cambridge, MA 02139

Abstract

Traditionally an earthquake is located by using the arrival times of P and S phases. This uses only a limited portion of the information on a seismogram. A large part of the information carried by the waveform is not used. In this study we investigate the applicability of the Time Reversed Acoustics (TRA) technique, and thus the whole waveform of the recorded signal, for earthquake locations and source characterization. The basic concept involved in TRA is the fundamental symmetry of time reversal invariance. Injecting the recorded signal, with time running backwards, reconstructs the whole wave field within the medium and can focus the wave field to the source. TRA has emerged as an important technique in acoustics with applications to medicine, underwater sound, and many other disciplines.

The objective of this paper is to demonstrate the feasibility of applying TRA to seismological data by means of simulating the relevant features using a finite-difference approach. The following subjects are investigated: (1) Locating the earthquake hypocenter; (2) finding the source space-time function; and (3) characterizing the direction of fault rupture during an earthquake. The results show that the TRA technique can focus back to the source reasonably well in a layered earth model and can recover the source time function. The results also show that TRA has a good tolerance to noise. For efficient applications, calculation time can be reduced by generating a medium response library. The source location and source time function can then be determined by convolving the medium response library with the time-reversed signals recorded at the seismic stations.

1. Introduction

Techniques based on the time reversal of wave fields are being investigated for applications in medicine for ultrasound target location, for material characterization in nondestructive evaluation and communication enhancement in oceanography. In TRA, the sound wave is first recorded in time, like an acoustic signal on a tape recorder, then re-emitted with time running backward, similar to playing the tape in reverse. An illustration is the time reversed mirror, which was demonstrated by Fink (1999). Imagine a sound signal being created by microphone array. Each microphone records the acoustic signal that arrives at its location and stores in a computer. The computer then reverses each signal and plays it back through the corresponding loudspeaker simultaneously with the other reversed signals. The sound field generated from the loudspeaker array would converge back to source.

The physical foundation of the TRA technique is rooted in the time reversal invariant of the wave equation. The governing equation used in wave propagation is:

$$\nabla^2 \psi + k^2 \frac{\partial^2 \psi}{\partial t^2} = 0 \,. \qquad (1)$$

In the equation, both the temporal and the spatial parts are second-order derivatives, which are self-adjoint in time and space, which satisfies the temporal and spatial reciprocity. In other words, if we record signals as a function of time at a boundary of a given region, then when the recorded signals were put back on boundary with time running backwards, the wave field in that region could be reconstructed within the medium. At some time the wave field is focused back onto acoustic sources inside.

This self-focusing property allows TRA to be applied in many areas. Several excellent reviews and theoretical articles have been written on the topic of TRA and its application, such as:
(1) underwater communication (Fink, 1993, 1997, 1999; Feuillade and Clay, 1992; Kupperman et al., 1998;

Hodgkiss et al., 1999; Song et al., 1999); (2) medicine (Hinkelman et al., 1994; Thomas et al., 1996); (3) nondestructive evaluation of materials (Fink, 2000). Some numerical analyses were developed to simulate the behavior of TRA (Borcea et al., 2002; Delsanto et al., 2002), and some experimental studies have been carried out (TenCate et al., 2003).

It is possible to apply TRA to seismology and related fields. In fact, the concept of time-reversal invariance has already been used in the petroleum industry, where it is known as time reversed migration. Using a two way time reverse finite difference migration, one can obtain accurate results for complicated structures (Claerbout, 1976; Kosloff et al., 1983; Whitmore, et al., 1983; Levin, 1984; Willis et al., 1986; McMechan et al., 1987).

To our knowledge, TRA has not been applied to seismic source location and source characterization problems. Traditionally, an earthquake is located by using the arrival times of P and S phases, which represents a limited portion of information on the seismogram, while a large amount of information that the waveforms carry are not fully used. In this study, several synthetic TRA experiments are presented and some basic characteristics of TRA are simulated using the finite different approach to study the applicability of TRA in a layered earth model. This forms the basis of our discussion on potential applications of TRA.

2. Methodology

We use a finite difference approach for wave propagation to model TRA. The finite difference method is used to solve partial differential equations by setting up a regular grid in space and time, and computing the approximate solutions on these grids by marching forward in time. It can incorporate general spatial variation models with elastic properties (Kelly, et al., 1976; Stephen et al., 1985; Virieux, 1986; Krasovec, 2004, personal communication).

From a signal processing aspect, wave propagation through a multiple scattering medium, just like any linear and time-invariant process, may be described as a linear system with a certain impulse response (Fink, 2000), as shown in Figure 1. Suppose the impulse response from the source to the j-th receiver is given by $h_j(t)$. Due to spatial reciprocity, $h_j(t)$ is also the impulse response from the j-th receiver to the source. In the first step the source excites a pulse $\delta(t)$, and the j-th transducer of the receiver array receives a signal $h_j(t)$. In the second step, the j-th receiver acts as a transmitter and sends out the time-reversed whole impulse response, which is $h_j(-t)$. This signal propagates through the medium and arrives at the source position as the convolution of $h_j(t)*h_j(-t)$. Supposing a N-element array, then the transfer function of such a two-step system can be written as

$$H(t)=\sum_{j=1}^{N} h_j(t)*h_j(-t)\,. \tag{2}$$

Therefore, given any kind of true source signal $s(t)$, the recreated signal at the source position due to a time-reversed mirror can be written as

$$s'(t)=s(t)*H(t)=s(t)*\sum_{j=1}^{N} h_j(t)*h_j(-t)\,. \tag{3}$$

In terms of signal analysis, $h_j(t)*h_j(-t)$ behaves as a matched filter. No matter what the impulse response $h_j(t)$, the convolution $h_j(t)*h_j(-t)$ has maximum value at time $t=0$, which is the correct time at which the source signal was excited. If some noise $n(t)$ gets added to the receiver array, then the back propagated signal becomes $h_j(-t)+n_j(t)$ and is retransmitted through the media, where $n_j(t)$ is the noise factor on the j-th receiver. The recreated signal can then be written as

$$s'(t)=s(t)*\left[\sum_{j=1}^{N} h_j(t)*h_j(-t)+\sum_{j=1}^{N} h_j(t)*n_j(t)\right]. \tag{4}$$

With the summation operation, the noise component is depressed due to the incoherence of noise.

3. Numerical Simulations

In the following 2- or 3-D simulation models, a medium is discretized with one or more sources and a set of receiver arrays (used both as the receiver at the recording stage and the transmitter at the time-reversed propagation stage) located at selected nodes. The size of the source is assumed to be small enough, compared to the wavelength, so that they can be treated as point sources or receivers. In the first step, a source signal of a given time function is applied on as a force vector. This includes two components in the 2-D case, $[v_x, v_z]$, (or three components in the 3-D case $[v_x, v_y, v_z]$) at corresponding node. The signals propagate through the medium and are captured by all the

elements of the receiver array. In the second step, every received signal is truncated, normalized, time-reversed, and reinjected by the corresponding element into the medium. During the back-propagation period, snapshots of the investigated medium (or part of it) are recorded to demonstrate the focus effects of TRA. In the following part, several models are constructed to simulate the TRA application. For simplicity, most models shown are 2-D.

(1) Circular Array Model

The first model is a 2-D circular array (with 61 receiver elements) within a layered earth structure, as shown in Figure 2. The radius of the array circle is 250m and the source is 50m off-centered. The dotted line limits a square area, in which the snapshots will be presented and discussed. The parameters for each layer (from top to bottom) are given in Table 1.

Table 1 Parameters of each layer

Thickness (m)	V_P (km/s)	V_S (km/s)	ρ ($\times 10^3$ kg/m^3)
150	3.00	1.70	2.6
250	4.00	2.00	2.2
250	4.20	2.50	2.1
150	3.40	2.00	2.3
200	4.80	3.20	2.6

A Ricker wavelet is used as the source time function, which is given by

$$s(t)=\frac{\sqrt{\pi}}{2}\cdot\left[\left(\frac{\omega_0 t}{2}\right)^2-\frac{1}{2}\right]\cdot e^{-\left(\frac{\omega_0 t}{2}\right)^2}, \quad (5)$$

where $\omega_0=2\pi f_0$, f_0 is the center frequency.

The source excites a signal and the receivers record it. The recorded waveforms at all the receivers are shown in Figure 3 (top). These waveforms are then truncated, normalized, and time-reversed, as shown in Figure 3 (bottom). Subsequently, each signal is reinjected into the medium using the corresponding receivers (each receiver acts as a source). During this reinjection period, consecutive snapshot of the observed region (as indicated by the dotted line in Figure 2) are captured. Examples of snapshots are shown in Figure 4, in which each row is a series of snapshots at a different time step. The top two rows are snapshots of the x-component and z-component, respectively. The bottom row is a snapshot of pressure, which is given as the summation of stress along the two axes. In the snapshots, green denotes zero-amplitude, blue denotes negative amplitude, and red denotes positive amplitude. The black dotted circle shows the position of the array. It is apparent that good spatial focusing can be observed on the fourth snapshot time step, Figure 4. The position of the focus lies exactly over the original source in the first step. If we plot the time response at the focal point (Figure 5 (bottom)), and compare it to the original source signal (Figure 5 (top)), we can see that the TRA can spatially focus back to the source location and recovers the source time function.

(2) Linear Array Model

In the circular array model, TRA was successfully simulated. However, in a real seismic recording situation, one cannot usually put the receivers into deep earth. Instead, the receivers are planted at the surface of the earth or buried along a surface at some depth. Therefore, it is necessary to investigate the TRA behavior if the receiver array is located along one side of the source, as shown in Figure 6. Again, the dotted line limits a square area where the snapshots will be presented and discussed.

In this model, the source is 250m below the receiver array. The receiver array on the surface has an aperture of 500m and includes 11 elements, with 50m spacing between the two. The parameters of the layered earth model are still the same as in the circular model, shown in Table 1. Following the same procedure, a series of snapshots are obtained. The snapshot at the focus time are plotted in Figure 8 (left). Although the snapshot results show good focus in space, the shape of the focus zone is less well-defined than the one in the circular array model. Comparing Figure 8 (left) to Figure 4, we can see that in the circular array model, the focal area is perfectly round. This is reasonable because the point source has a symmetric radiation pattern. In the linear receiver array model, however, the focal area is elongated with better focus along the x-axis but worse focus along the z-axis. The reason for this difference is

that while the circular array samples the wave field along the whole boundary surrounding the medium, the linear receiver array is positioned only at one side of the source along the x-axis. This gives better spatial constraint in the x direction and poor constraint in the z direction.

As seen in the circular array model above, to demonstrate the focus effect, we show a series of snapshots in x-z domain with respective to time. This enables us to judge at what time step the snapshot has the best focus. Due to human interaction, this focus picking method may have certain ambiguity. In order to automatically pick the right focus time and spatial focal zone, the 2-D spatial-time domain is separated into two 1-D spatial-time domains. The values in one snapshot along the z-dimension for each x position are summed, which makes the 2-D snapshot matrix into a 1-D vector. This 1-D vector indicates the energy distribution along x-axis. By doing this at each time step, it is possible to get a x-time domain distribution, as shown in Figure 7 (left). Since the array has better constraint along the x direction, we can observe a clear high amplitude area in the x-time domain plot. This area indicates the focus time and the focal position in x-axis. We can also do the same thing along the z-dimension, as shown in Figure 7 (right). We can see that because the constraint along the z direction is very weak, the energy distribution forms a linear pattern. This means that the energy propagates along the z direction with time. To obtain the z position of focal zone, we can draw a horizontal line at the focus time, which is already obtained from Figure 7 (left). The cross point of this time line and the energy distribution line gives the z position, which is also the maximum point along the time line.

Figure 8 (right) shows the comparison of the recovered signal and the original source signal. It is obvious that the source time function can be recovered well even though the TRA has some limitation on focus positioning in this case.

(3) Factors Affecting Focal Resolution

In this section we investigate the relationship between focal resolution and different factors in the model. The first experiment compares the resolution with differing combinations of wavelength and array element spacing at the same array aperture. Keeping the same array aperture as shown in Figure 6, the number of receivers and the distance between two receivers are changed, as shown in Figure 9. In this model, two different arrays are used. One with 21 receivers evenly spaced from $x=-250$ to $x=250$ and another with 6 receivers covering the same area. Figure 10 (left) and (center) are snapshot results from these two arrays, both of them excite at the same signal frequency. We can observe that the snapshot with 21 receivers has less "smile" trailer energy than the one with fewer receivers. This is reasonable because the more signals that are reinjected into the region, at the focus time step, the more the displacement can cancel out at grid points that are not the focus. Therefore the reconstructed field is more approximate to the true wave field at that time. Although the case with more receivers has cleaner background, the focus and resolution are almost the same in this two cases. In another result, as shown in Figure 10 (right), again uses 6 receivers but the signal wavelength is now half of the one in Figure 10 (left) and (center). The focal area shrinks to almost half of the focal area in Figure 10 (left) and (center). We can see that given the same array aperture, a high frequency wave gives better resolution while increasing array elements does not improve the resolution much.

The second experiment is designed to determine the ability of TRA to distinguish two sources, and relate it to the resolution of the array. In this experiment, two point sources are placed at the same depth and excited at the same time, as shown in Figure 11. The distance between two sources changed from half the wavelength to two wavelengths. In Figure 12 (left), two sources are separated at about $\lambda/2$. The focal zones of two sources overlap with each other and it is impossible to distinguish the two sources. In Figure 12 (center), the distance increases to about 1λ. Now both sources can be recognized but they still overlap a little. As the distance continues increasing to 2λ, as shown in Figure 12 (right), the two sources can be completely and clearly separated by TRA.

The effective aperture of the array also has a big impact on the ability of refocusing back to the source. Three models with the same number of receivers but with different array apertures are designed to investigate this problem, as shown in Figure 13. All the three arrays contain the same number of receivers, but the distance between two neighboring receivers varies, thus changing the array aperture. The source is positioned away from the symmetric axis so that it is covered by the array #1, on the edge of the array #2, but outside the coverage of the array #3. Figure 14 shows the results from the three models, respectively. We can see the focus effect worsens when the source moves outwards from the array's coverage. The reason comes from the horizontal constraint provided by the array. If the source is outside of the array, the receivers will only sample one side of the wave field, thus the constraint along the x direction becomes as weak as along the z direction.

These results show both the limitation and promise of the TRA application to seismic data. The limitation is that the resolution is highly dependent on the wavelength. Since the wavelength is given by the wave speed divided by the frequency, the resolution is good at high frequiencies . The success of the TRA also depends on the aperture coverage of the receivers array. However, given the region and the seismic wave frequency range to be investigated,

it is not necessary to set up a densely spaced array as long as the array has enough coverage over the region. This is beneficial from an economic aspect.

Another advantage of the TRA technique is noise tolerance. This can be simulated numerically. After the array records the signal from the source, Gaussian random noise is added to the original signal, as shown in Figure 15. Then the contaminated signal is time-reversed and reinjected back into the region. Figure 16 shows a comparison between the snapshot result from the original signal (Figure 15 (left)) and the noisy signal (Figure 15 (right)). A noisy background is observed in Figure 16 (right), however the noise level is low enough to pick up the main focus position. Furthermore, the signal to noise ratio is fairly good in the recovered source time function, as shown in the comparison in Figure 17. We compare this to the one recovered using the original recorded signal. It is evident then that the recovered signal with noise still preserves the most useful information about the source function.

(4) Fault Simulation

One of the big challenges in earthquake focal mechanism studies is to determine the fault plane and the auxiliary plane. This might give rise to a possible application of TRA – fault rupture direction detection. We simulate the fault rupture by a series of point sources located on a dipping fault plane, with time delay between adjoining sources corresponding to rupture velocity, as shown in Figure 18. The time delay between the two point sources is given by $\Delta t = \Delta d / 0.8 V_S$, where Δd is the distance between two point sources and V_S is the shear wave speed. A moment tensor source is applied for each source point to simulate the fault mechanism. This is given by

$$M_{jk} = \lambda \delta_{jk} v_m e_m + \mu (v_j e_k + v_k e_j), \tag{6}$$

where $\vec{v}$ is the normal direction cosine of the fault plane and $\vec{e}$ is the direction cosine of the slip direction. The simulation results, shown in Figure 19, are for fault planes with different dip angles. It shows that the TRA technique tracks the fault plane and rupture direction well.

4 Medium Response Library

With the finite difference approach, the TRA process is easy to implement. The biggest disadvantage of the finite difference approach is the computational expense. To avoid this problem, a medium response library concept is introduced. For a given medium, the region is gridded and the transfer function (also referred as the Green's function) between the stations and grid points within the region are calculated. A medium response library matrix is then constructed based on these relationships. There are many methods to obtain the transfer function between the grid point inside the region and the station. One of the methods is to use a test wavelet to get the transfer function between the station and the grid points inside the region. Suppose there are N stations and M grid points. Applying a test signal $\mathbf{f} = [f_x, f_y, f_z]$ on the n-th station, we can calculate the response at the m-th grid point. For example, the z-component response at the m-th grid point due to the x-component of the test signal f_x is given as $g_{xz}^{[n,m]} = f_x * h_{xz}^{[n,m]}$, where $h_{xz}^{[n,m]}$ is the transfer function between the x-component at the n-th station and the z-component response at m-th grid point. $g_{xz}^{[n,m]}$ can be calculated using the finite difference approach (or other methods like discrete wavenumber method), then $h_{xz}^{[n,m]}$ can be obtained by deconvolving f_x from $g_{xz}^{[n,m]}$. Calculating this for all the stations and grid points for all components, we can setup an $N \times M$ response matrix between all stations and all grid points:

$$\Xi = \begin{bmatrix} \mathbf{H}^{[1,1]} & \mathbf{H}^{[1,2]} & \cdots & \mathbf{H}^{[1,M]} \\ \cdots & \cdots & \cdots & \cdots \\ \mathbf{H}^{[N,1]} & \mathbf{H}^{[N,2]} & \cdots & \mathbf{H}^{[N,M]} \end{bmatrix}, \tag{7}$$

in which each element is a small response matrix given by

$$\mathbf{H}^{[n,m]} = \begin{bmatrix} h_{xx} & h_{xy} & h_{xz} \\ h_{yx} & h_{yy} & h_{yz} \\ h_{zx} & h_{zy} & h_{zz} \end{bmatrix}^{[n,m]}. \tag{8}$$

When seismic signals are recorded ($\mathbf{s} = [s_x, x_y, s_z]$), the source location and source time function can be determined quickly. Instead of injecting the time-reversed signals into the region and run finite difference, we can simply convolve the medium response library matrix with the time-reversed signals recorded on the seismic stations. The recovered signal at the m-th grid point due to the recorded signal at the n-th station can then be written as:

$$
\begin{aligned}
[r_x, r_y, r_z]^{[n,m]} &= \mathbf{s}^{[n]} * \mathbf{H}^{[n,m]} \\
&= [s_x, s_y, s_z]^{[n]} * \begin{bmatrix} h_{xx} & h_{xy} & h_{xz} \\ h_{yx} & h_{yy} & h_{yz} \\ h_{zx} & h_{zy} & h_{zz} \end{bmatrix}^{[n,m]} \\
&= \left[s_x^{[n]} * h_{xx}^{[n,m]} + s_y^{[n]} * h_{yx}^{[n,m]} + s_z^{[n]} * h_{zx}^{[n,m]},\ s_x^{[n]} * h_{xx}^{[n,m]} + s_y^{[n]} * h_{yx}^{[n,m]} + s_z^{[n]} * h_{zx}^{[n,m]},\right. \\
&\qquad \left. s_x^{[n]} * h_{xx}^{[n,m]} + s_y^{[n]} * h_{yx}^{[n,m]} + s_z^{[n]} * h_{zx}^{[n,m]} \right]
\end{aligned} \tag{9}
$$

The summation of $[r_x, r_y, r_z]^{[n,m]}$ for all the N stations gives the final recovered signal at that grid point.

$$
[r_x, r_y, r_z]^{[m]} = \sum_{n=1}^{N} [r_x, r_y, r_z]^{[n,m]} . \tag{10}
$$

Comparison shows that for the same number of grid points in a 3-D model, with the same computational ability, the medium library response approach uses at least 75 times less calculation time than the finite difference approach. Furthermore, the response library matrix only needs to be constructed once, thus this approach is especially useful if there are frequent earthquake events occurring within a region. Since the monitored area is known, once the library is constructed, the source location and source time function can be monitored easily and quickly. This might be very useful in real-time reservoir monitoring.

Another advantage of introducing a response library is that we can set up an inversion scheme, based on TRA, for the earth model parameters. Suppose we have a fairly good estimate or prior knowledge of the source position and a set of seismic signals due to that source are recorded at several stations on surface. The Green's function between stations and the grid points in a small region neighboring the source can be calculated by introducing an earth model, which is also a medium response library. Using the algorithm above, the snapshot in that neighboring region can be obtained by a simple convolution operation. The source position can then be determined automatically using techniques as shown in Figure 7. The objective is to minimize the difference between the inversed source position and the well-estimated position.

5. Earthquake Location – A Test with Field Data

In this section, an application of TRA to seismic event location is shown with actual field data. Data are seismic recordings from small earthquake at Yibal, Sultanate of Oman, provided by Petroleum Development Oman, LLC. Five seismic stations are distributed on the surface, as shown in Figure 20. The triangles denote the stations positions. The five stations are numbered from #1 to #5, and the coordinate system is constructed with the #5 station being at the origin. A 1-D velocity profile of this region is shown in Table 2.

Table 2 1-D velocity profile of Yibal gas reservoir

Thickness (km)	V_P (km/s)	V_S (km/s)	ρ ($\times 10^3$ kg/m^3)
0.25	2.30	1.198	2.74
0.65	2.60	1.354	2.74
0.60	3.30	1.719	2.74
1.50	4.50	2.344	2.74
4.00	5.10	2.656	2.74
7.00	5.80	3.021	2.74
16.00	6.60	3.438	2.74
30.00	8.00	4.167	2.74

Each station records the three components of ground motion. We used one event to do the TRA experiment. The three component waveforms recorded at five stations for this event are shown in Figure 21. To reduce the calculation time and to make a comparison, the source location was determined first using the P arrival times and HYPO program (shown as the star point in Figure 20). Based on this prior knowledge, a cube with the x-axis from -510m to 2010m, the y-axis from -3000m to 480m and the z-axis from 990m to 2970m is discretized into

60×60×60 m grids, and response at these grid points are calculated. Figure 22 is a snapshot slice in X-Y plane at one possible depth z=2370m, which is determined based on the HYPO result. The maximum energy is at about x=1200m, y=-750m, which is denoted as the circle in Figure 20. Compared to the HYPO result, the TRA epicenter moved towards northeast by about 1.2km.With the limited data it is difficult to identify the reason for this difference. We do not know the error ellipse of the HYPO location. In the TRA case, we are not sure how much error comes from using only five stations. Although five stations may be enough in a 2D case, the data coverage is very sparse for a 3D investigation. It is also possible that the velocity model has deviation from the true value. A well-positioned calibration event will be much helpful for testing the TRA method.

6. Conclusions

In this paper, the feasibility of applying TRA to the seismologic data is demonstrated. Numerical simulations show that the TRA technique can successfully locate a seismic source inside the earth, such as an earthquake, explosion, etc. It can also recover the source time function. The method has fairly good tolerance to noise. Synthetic results also show that it is possible to use TRA to determine the fault dip and rupture direction, important application in seismology. In order to improve TRA efficiency, the concept of constructing a medium response library is introduced and evidence shows that with the library approach, the process time decreased by a factor of 75, making this technique a step closer to real applications.

Although numerical simulation shows that the TRA technique has great potential, it also has some limitations. One limitation is that the resolution is constrained by the wavelength. For high resolution, high frequency data are needed. Other limitation include array geometry and array aperture.

The preliminary results with field data show that, although there are still problems with the TRA application to field data, it is encouraging that the focusing effect can be observed with a sparse station distribution.

7. Acknowledgment

This work was supported by the Earth Resources Laboratory Founding Member Consortium.

References

Borcea, L., and Papanicolaou, G. (2002), Imaging and time reversal in random media, Inverse Problem, 18:1247-1279

Chang, W., and McMechan, G. (1987), Elastic reverse-time migration, Geophysics, 52:1365-1375

Claerbout, J. (1976), Fundamentals of geophysical data processing, New York, McGraw-Hill Book Co. Inc.

Delsanto, P., and Johnson, P. (2002), LISA simulations of time-reversed acoustic and elastic wave experiments, J. Phys. D, 35:3145-3152

Feuillade, C., and Clay, C (1992), Source imaging and side-lobe suppression using tie-domain techniques in shallow water waveguide, J. Acoust. Soc. Am., 92:2165-2172

Fink, M. (1993), Time reversal mirror, J. Phys. D, 26:1330-1350

Fink, M. (1997), Time reversed acoustics, Phys. Today, 50:34-40

Fink, M. (1999), Time reversed acoustics, Scient. Am., 281:91-97

Fink, M., and Cassereau, D. (2000), Time reversed acoustics, Rep. Prog. Phys., 63:1933-1994

Hellman, K., and Willis, M. (1986), Evaluation of a Reverse-Time Prestack Migration Algorithm, Presented at the

56th Ann. Internat. Mtg., Sot. Explor. Geophys.

Hinkelman, L., and Liu, D. (1994), Measurements of ultrasonic pulse arrival time and energy level variation produced by propagation through abdominal wall, J. Acoust. Soc. Am., 95:530-541

Hodgkiss, W., and Song, H. (1999), A long range and variable phase conjugation experiment in shallow water, J. Acoust. Soc. Am., 105:1597-1604

Kelly, K., and Ward, R. (1976), Synthetic Seismograms: A Finite Difference Approach, Geophysics, 41:2-27

Kosloff, D. D, and Baysah, E. (1983), Migration with the full acoustic wave equation, Geophysics, 48:677-687

Kupperman, W., and Hodgkiss, W. (1998), Phase conjugation in the ocean: experimental demosntration of an acoustic time reversal mirror, J. Acoust. Soc. Am., 103:25-40

Levin, S. (1984), Principle of reverse-time migration, Geophysics, 49:581-583

Song, H., and Kuperman, W. (1999), Iterative time reversal in the ocean, J. Acoust. Soc. Am., 105:3176-3184

Stephen, R., and Casas, C. (1985), Finite differece synthetic acoustic logs, Geophysics, 50:1588-1609

Sutin, A., Johnson, P., and TenCate, J. (2003), Developement of nonlinear time reversed acoustics (NLTRA) for applications to crack detection in solids, Presented at World Congress of Ultrasonics 2003, Paris

Thomas, J., and Wu, F. (1996), Time reversal focusing applied to lithotripsy, Ultrason. Imag., 18:106-121

Virieux, J. (1986), P-SV wave propagation in heterogeneous media: Velocity-stress finite difference method, Geophysics, 51:345-369

Whitmore, N. (1983), Iterative depth migration by backward time propagation, Presented at the 53rd Ann. Internat. Mtg., Sot. Explor. Geophys.

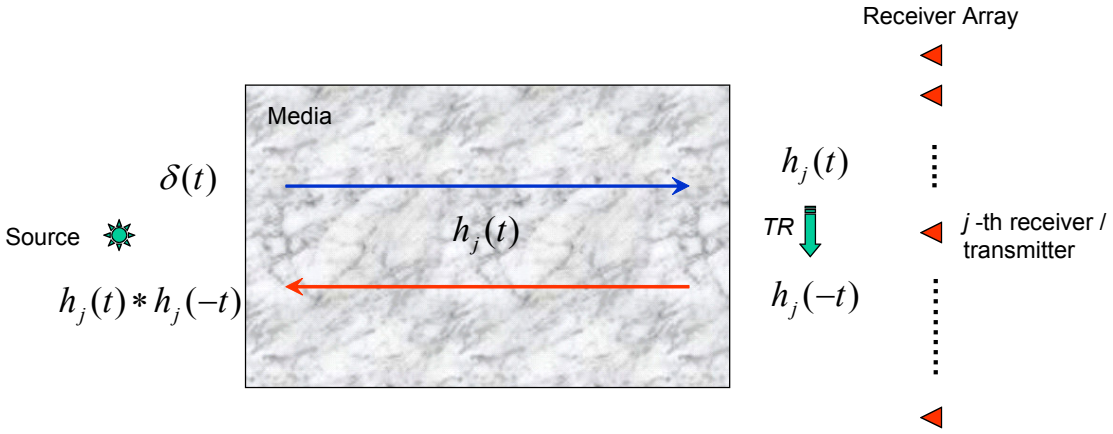

Figure 1. Illustration of time reversed acoustics.

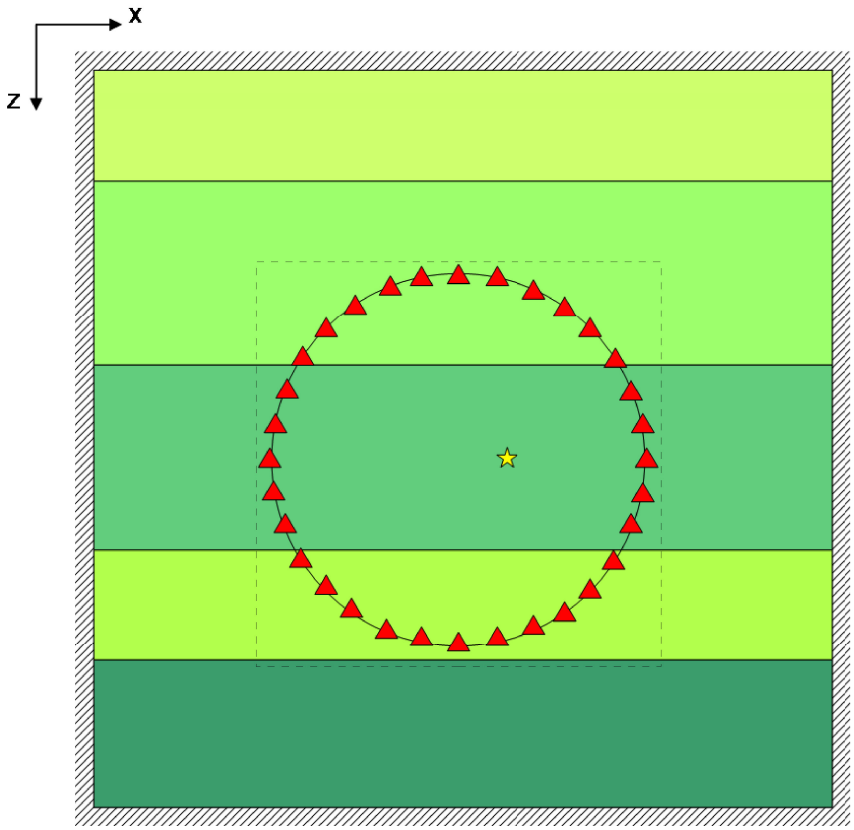

Figure 2. Circular array with layered earth model.
Dotted line limits the region where snapshot will be discussed.

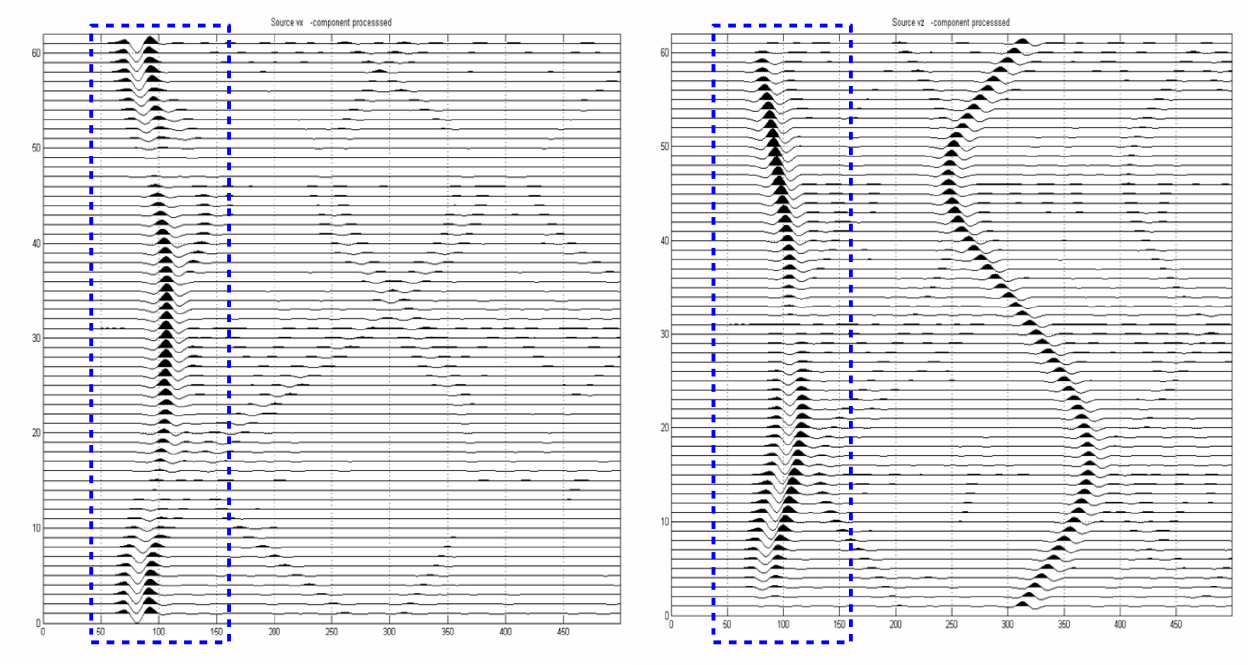

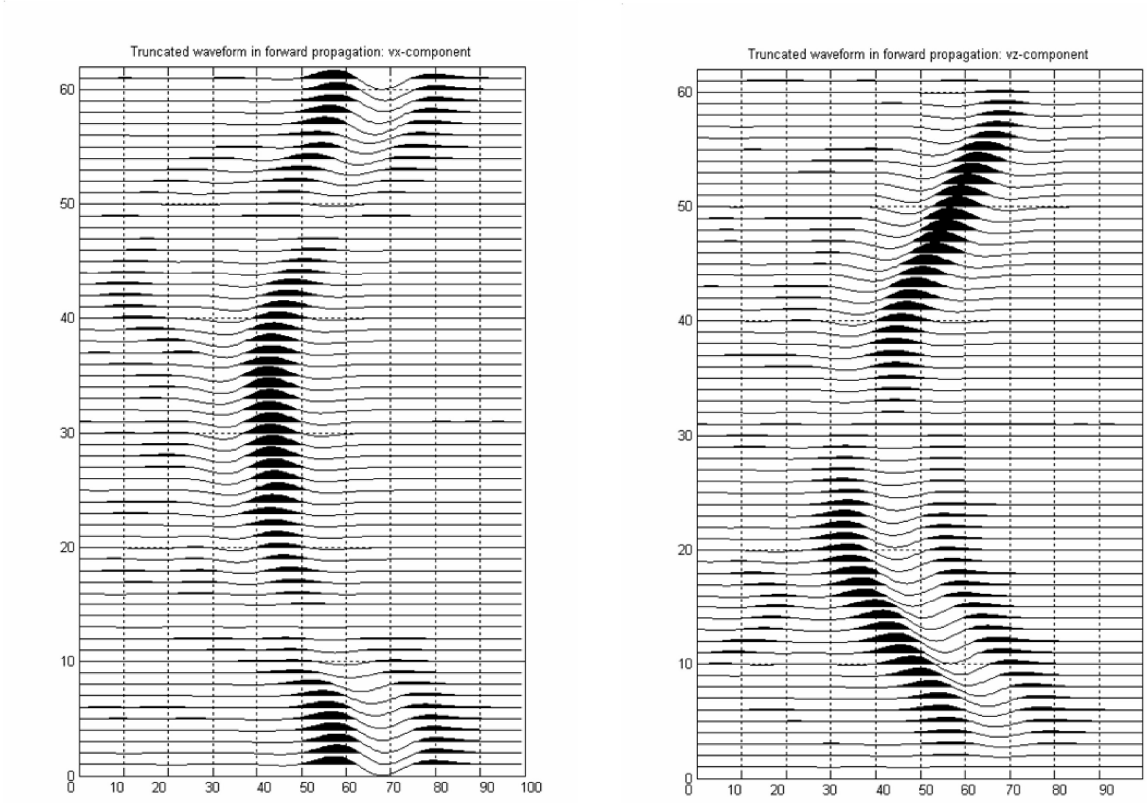

Figure 3. Recorded traces at the receivers.
Top: whole wave signal recorded at the all the receivers, waveforms in dashed box are truncated; Bottom: truncated and time-reversed signal at the all the receivers.
Left: x-components; Right: z-components.

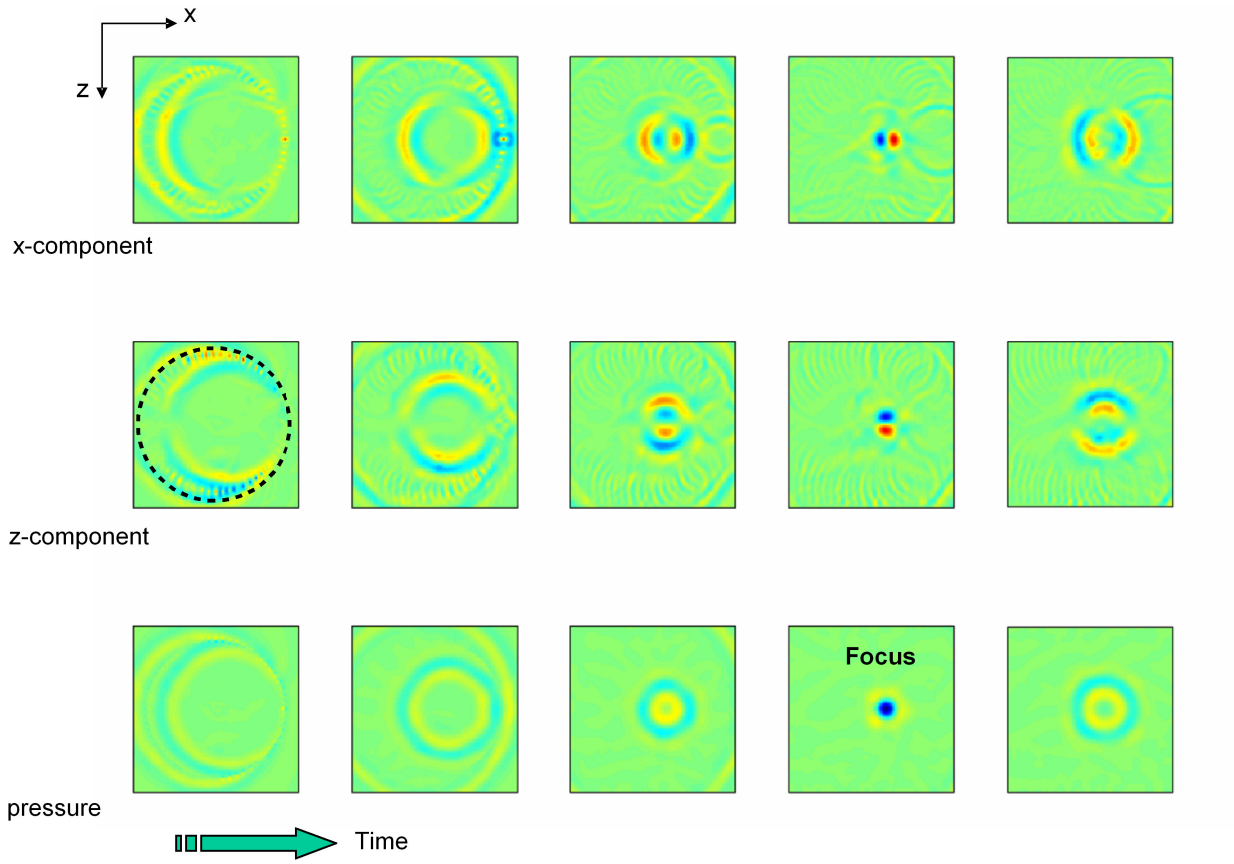

Figure 4. Circular array model back-propagation snapshots.

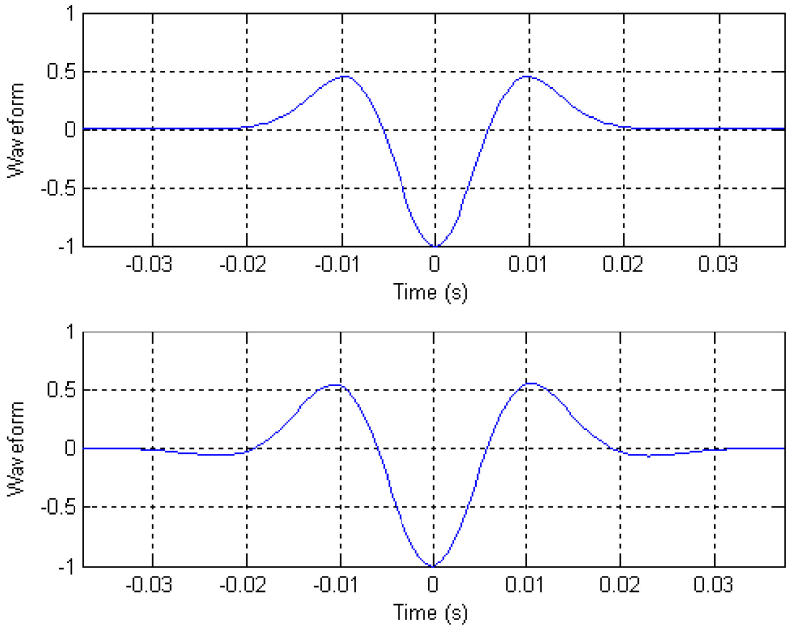

Figure 5. Comparison between original source time function (top) and recovered signal waveform (bottom) at the source position.

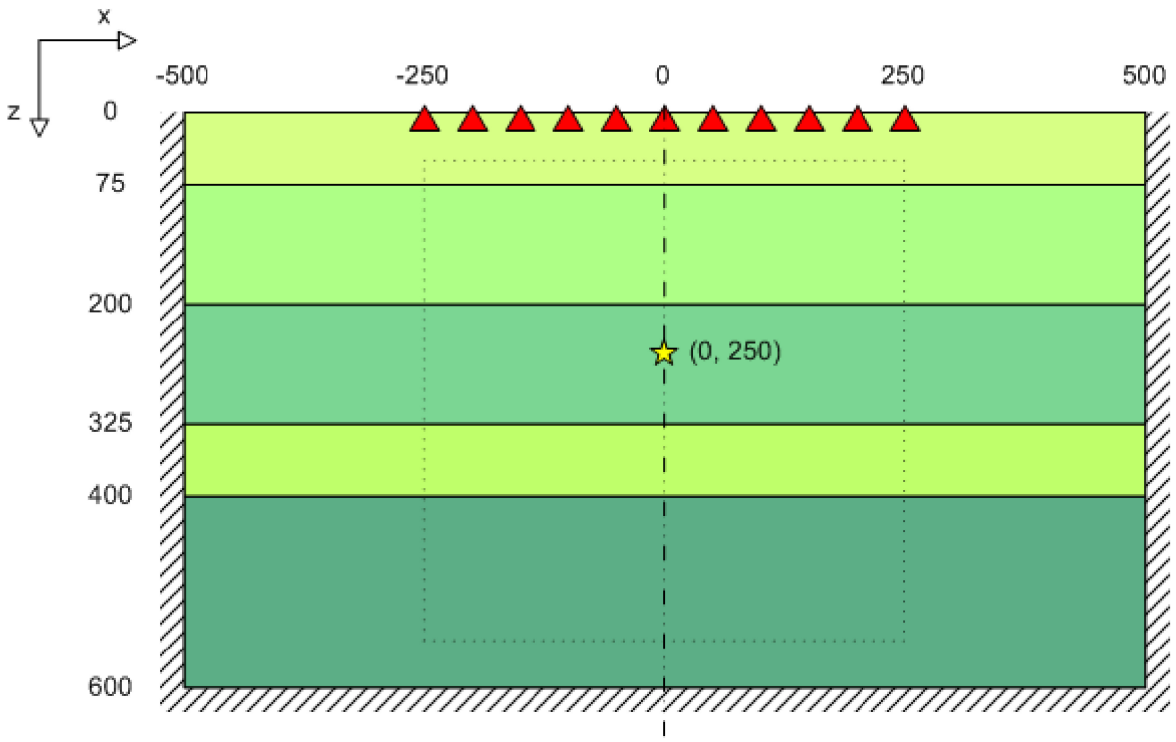

Figure 6. Linear receiver array within a layered earth model.

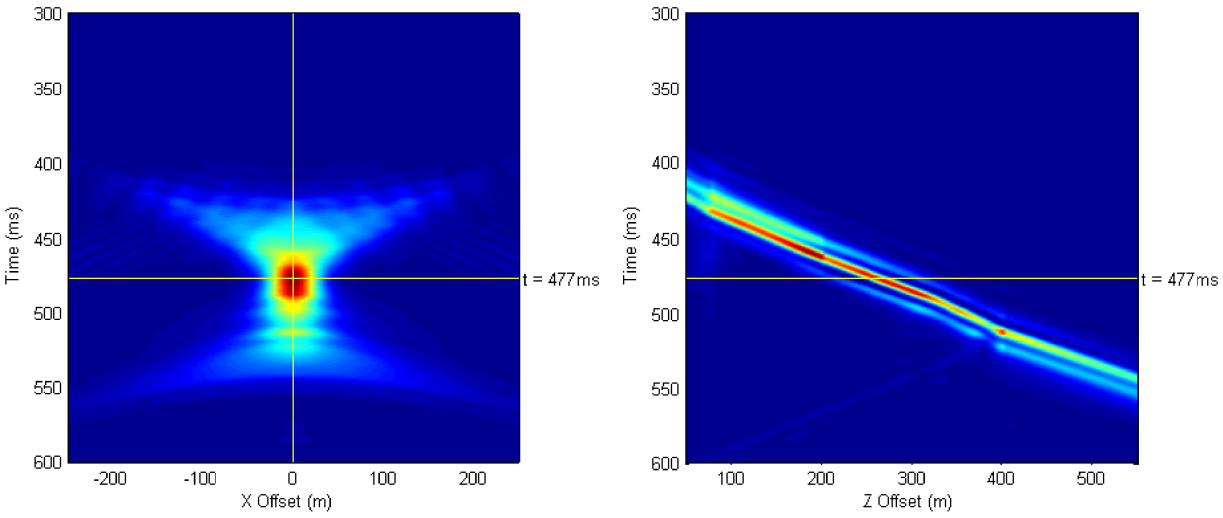

Figure 7. Method to find the focus point in time and space.

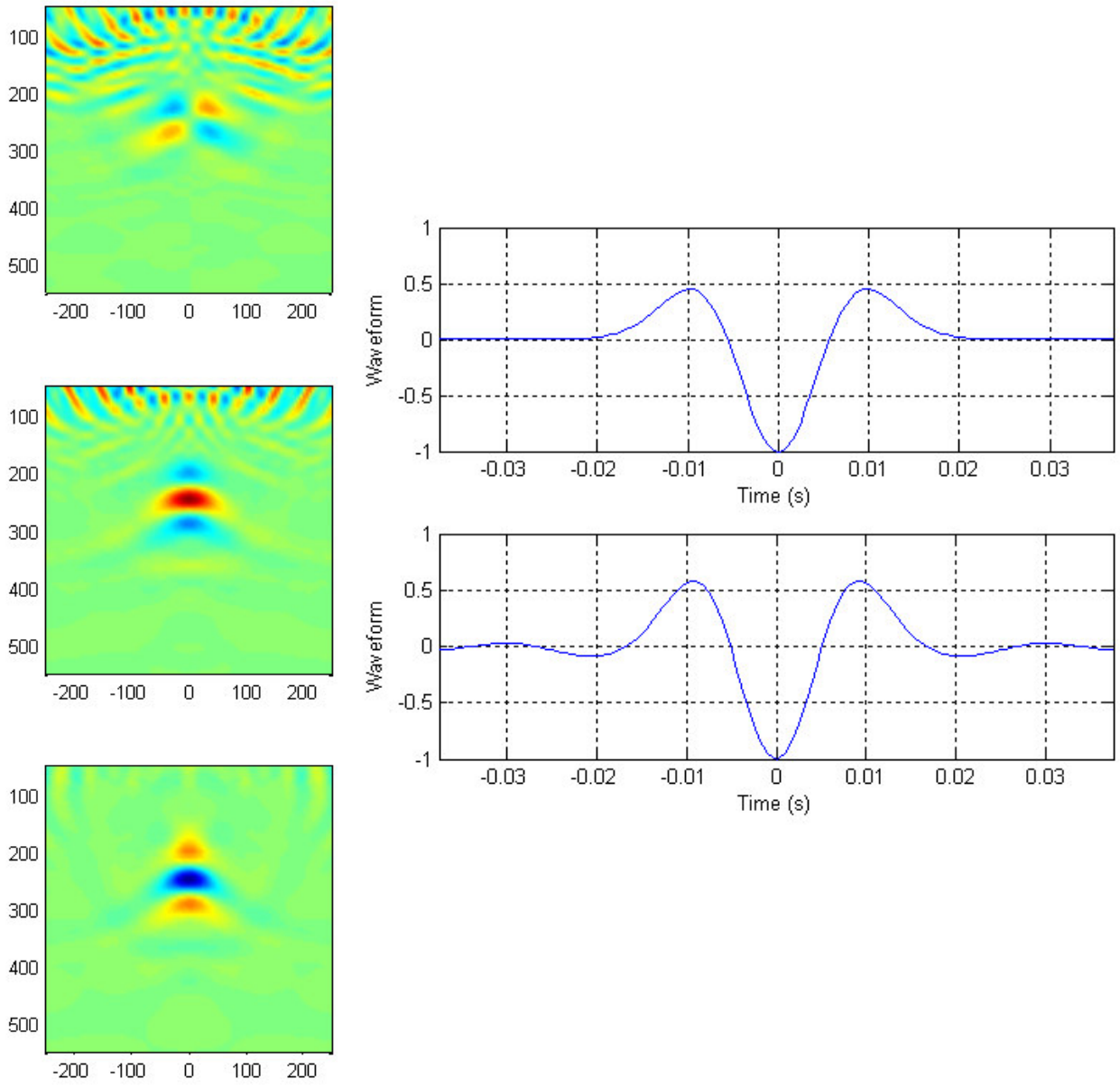

Figure 8. Snapshot results (left) and waveform comparison at the focus zone (right) in the linear receiver array model

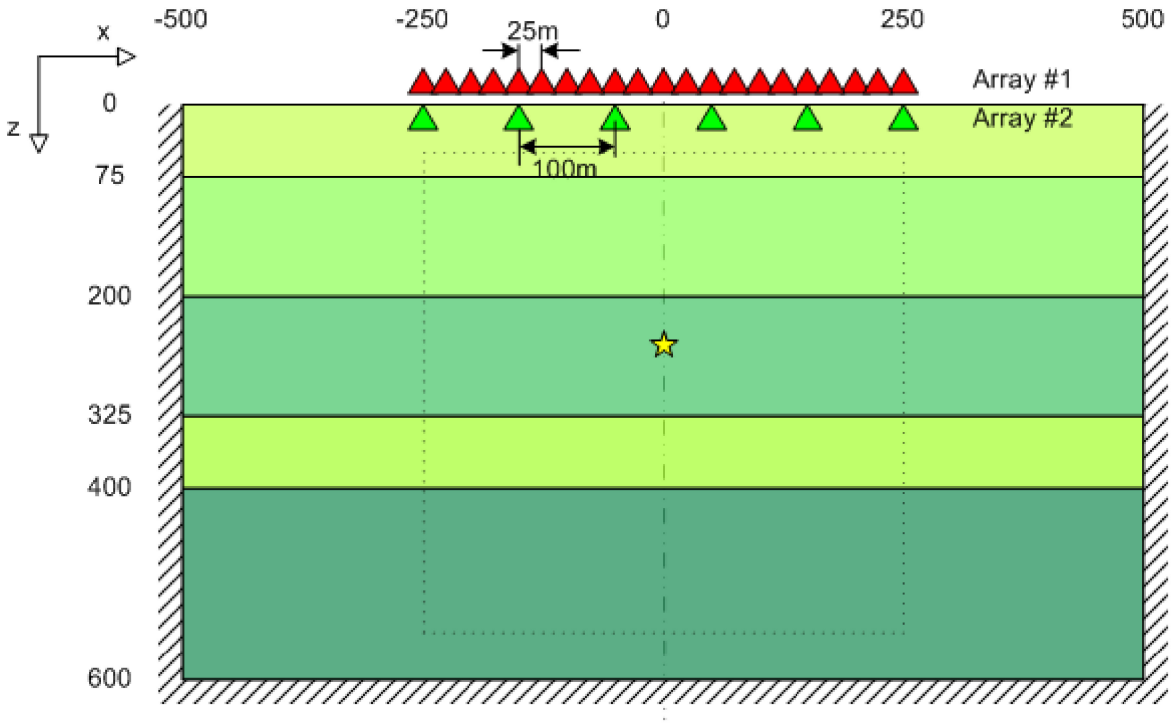

Figure 9. Model of two sets of array with different number of elements at the same aperture.

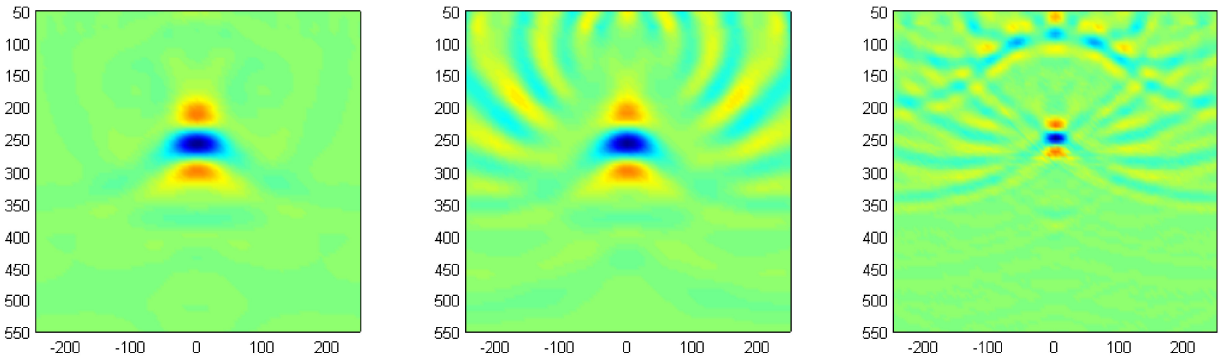

Figure 10. Snapshot results comparison at different combinations of wavelengths and array elements spacing at the same array aperture
Left: 21 receivers, 40Hz; Center: 6 receivers, 40Hz; Right: 6 receivers, 80Hz

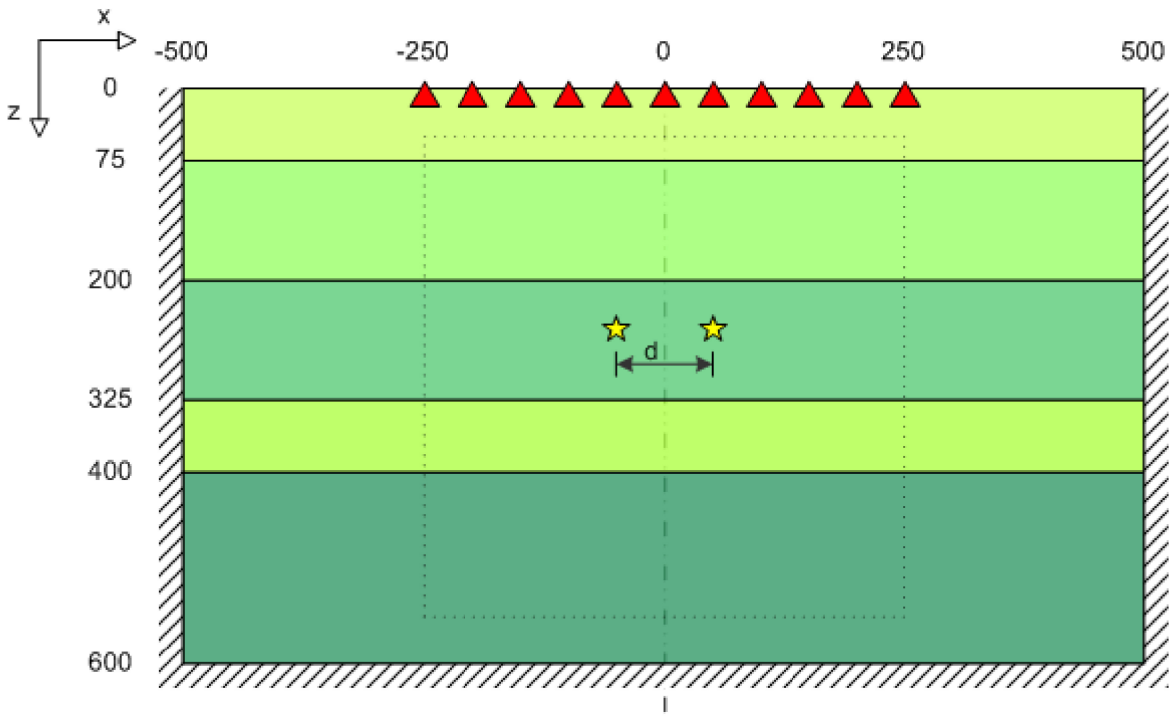

Figure 11. Model of two sources separated at different distance.

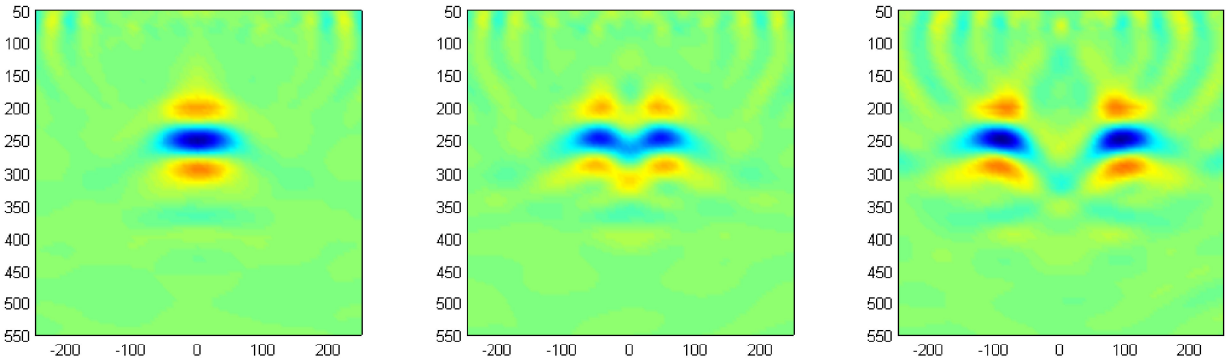

Figure 12. Snapshot results comparison for different source distance at the same array aperture. Left: ½ wavelength apart; Center: 1 wavelength apart; Right: 2 wavelength apart

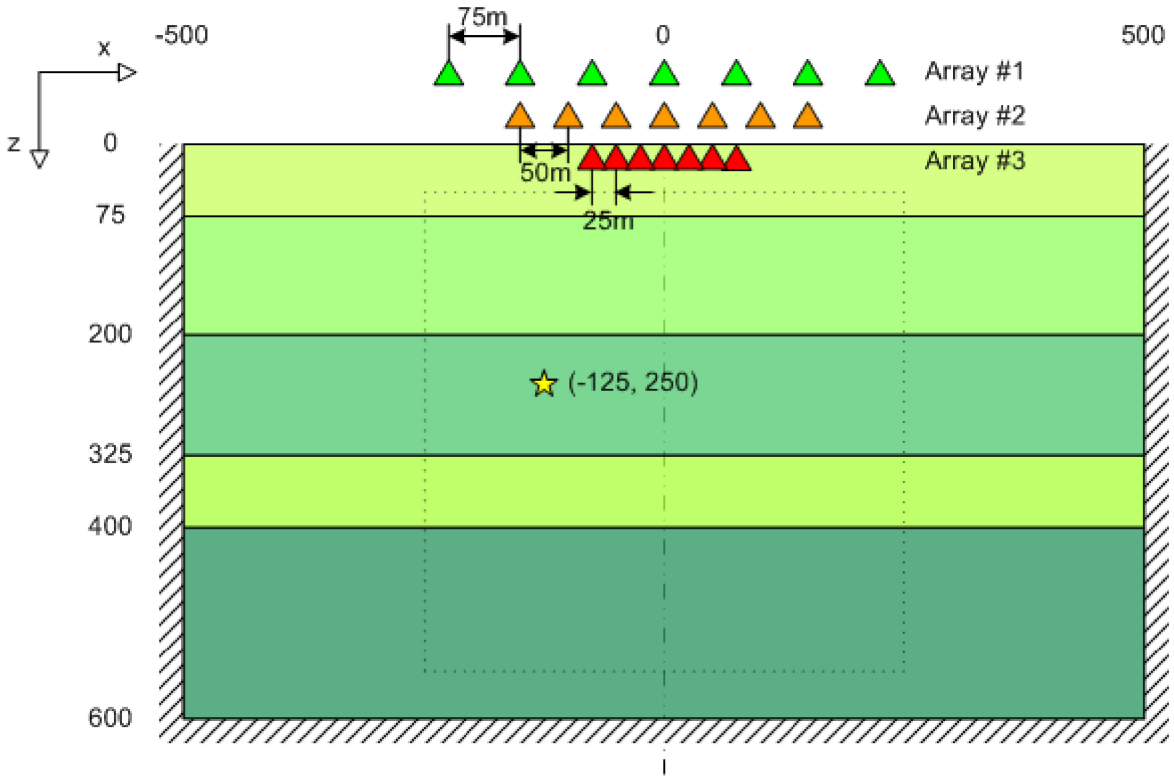

Figure 13. Model of three set of arrays with same number of receivers but different effective apertures. The source is off-centered.

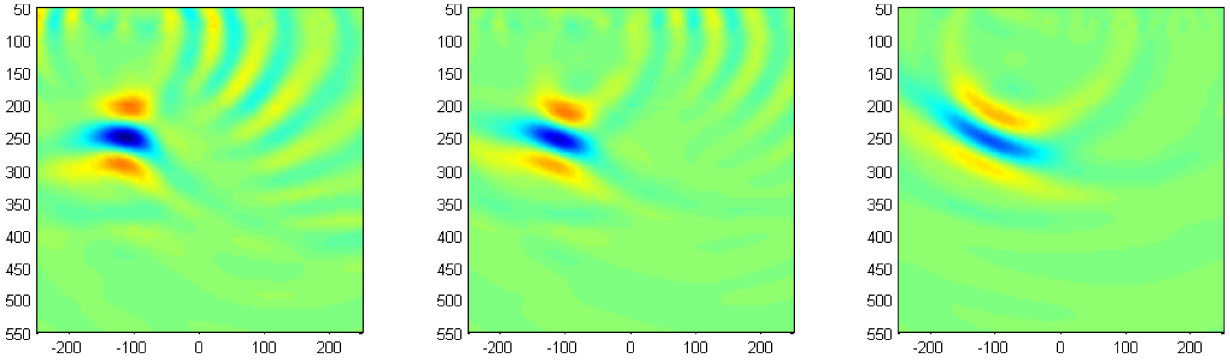

Figure 14. Snapshot result for different effective array aperture.
Left: under coverage, array #1;
Center: on edge of coverage, array #2;
Right: out of coverage, array #3.

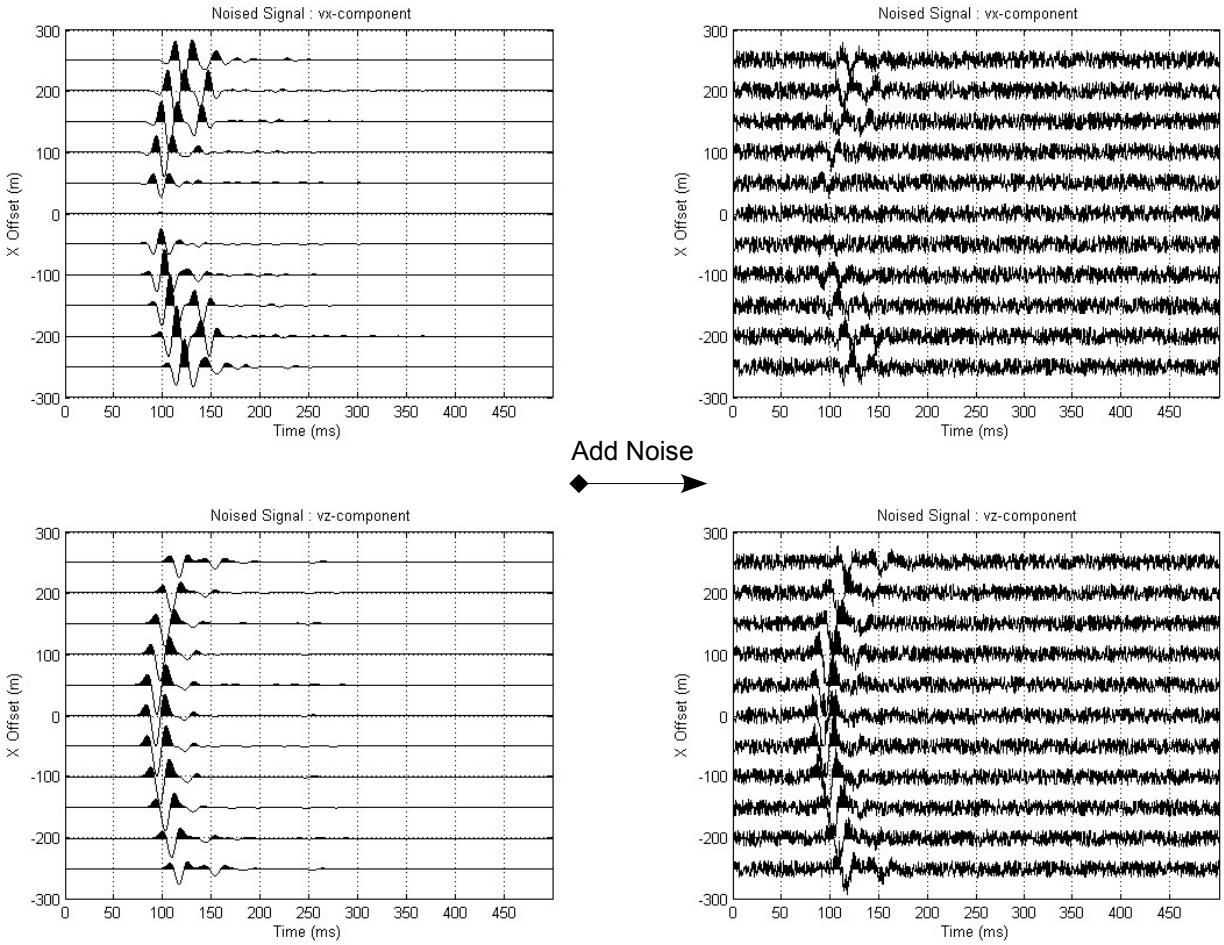

Figure 15. Recorded signal in the TRA first step, before and after adding noise.

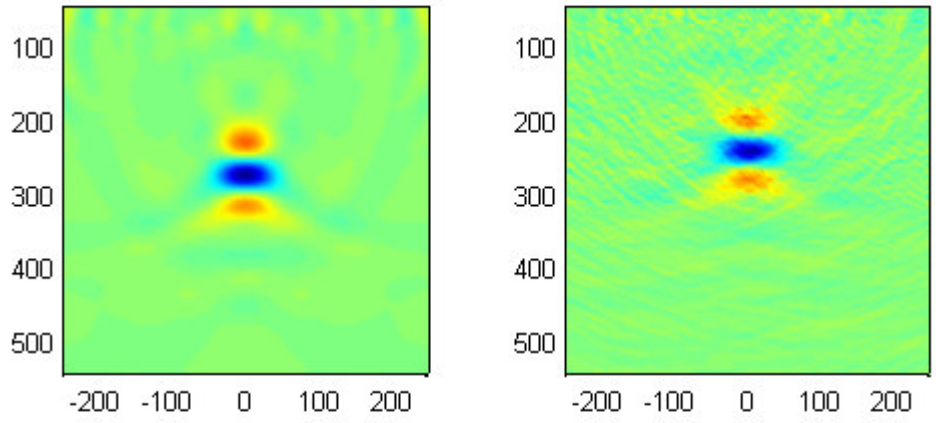

Figure 16. Snapshot comparison at focal area
using the noise-contaminated signal during the back-propagation step.

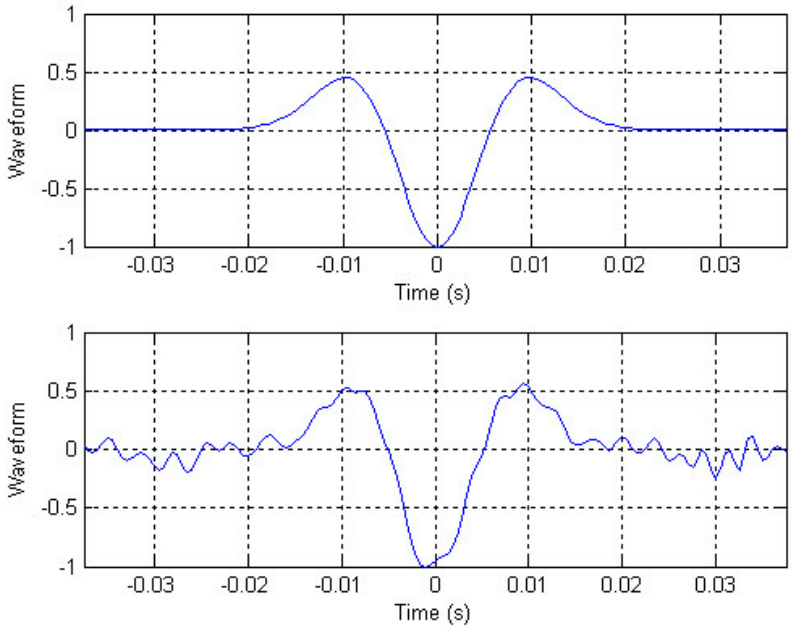

Figure 17. Recovered waveform at focus
Top: original source signal; Bottom: recovered signal from a noise-contaminated signal during the back-propagation step.

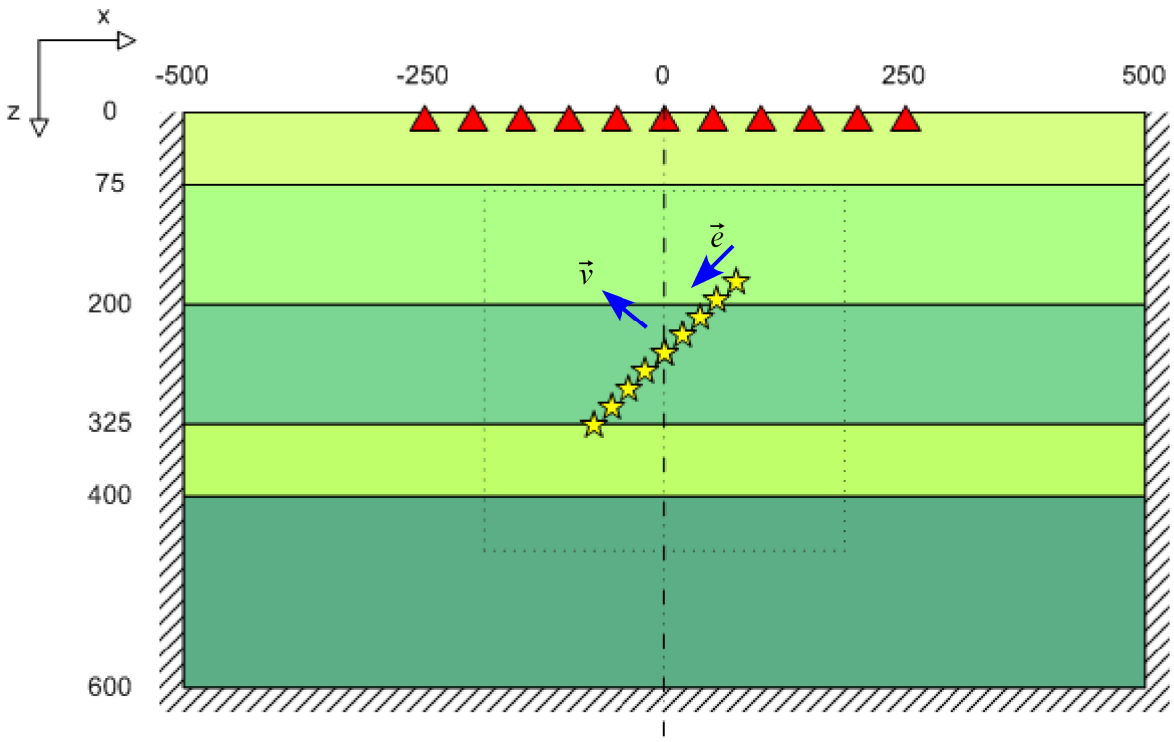

Figure 18. Fault rupture simulated by a series of point sources.

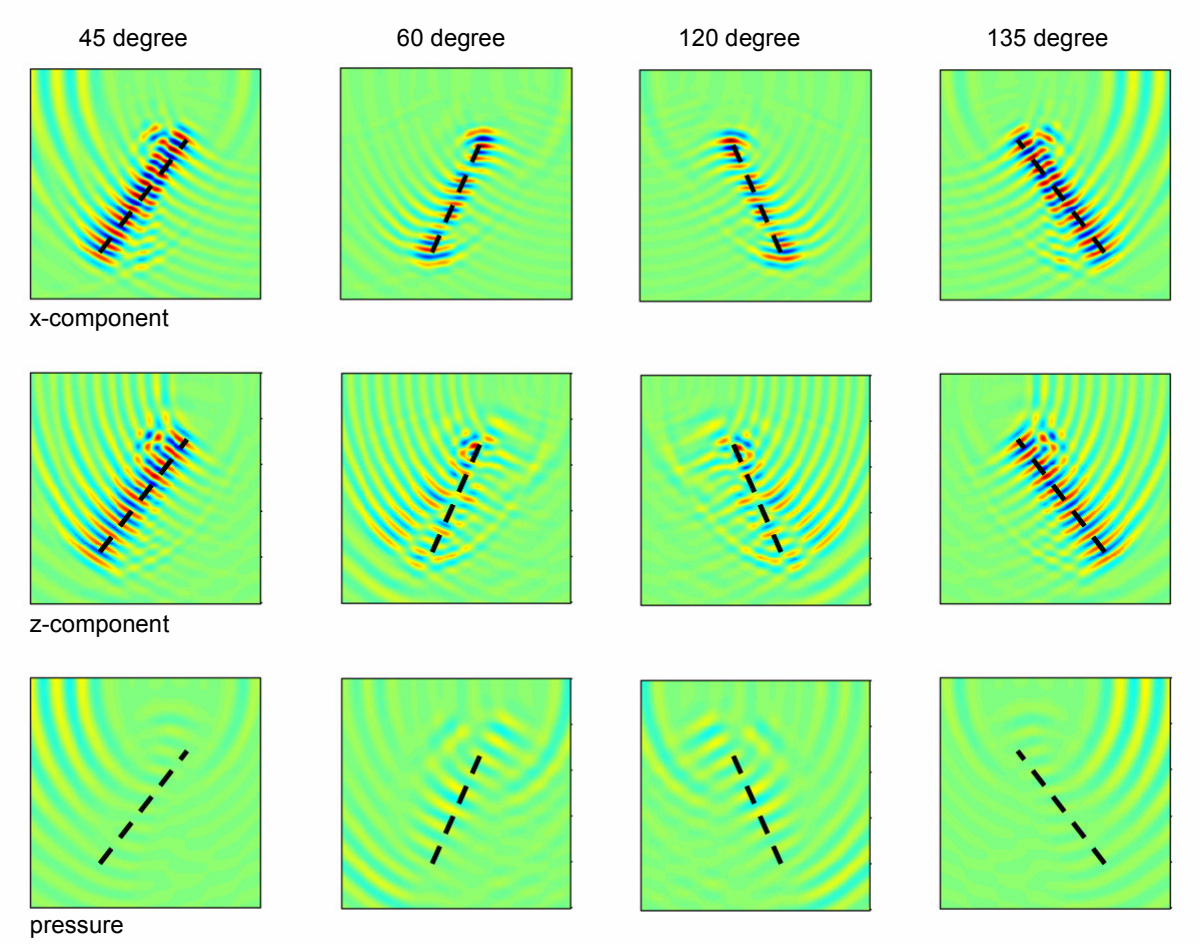

Figure 19. Fault simulation snapshot results of different fault plane dip angles.

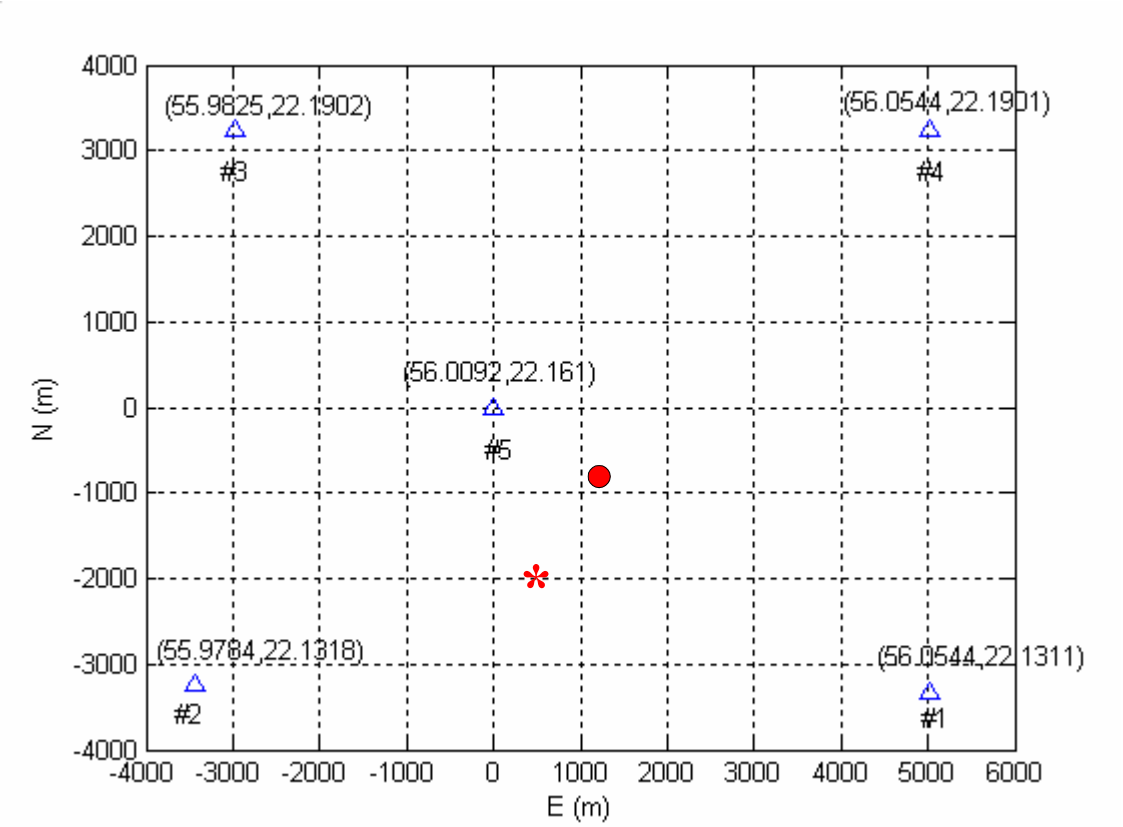

Figure 20. Yibal field seismic network.
Star denotes the source position given by HYPO; Circle denotes the position given by TRA

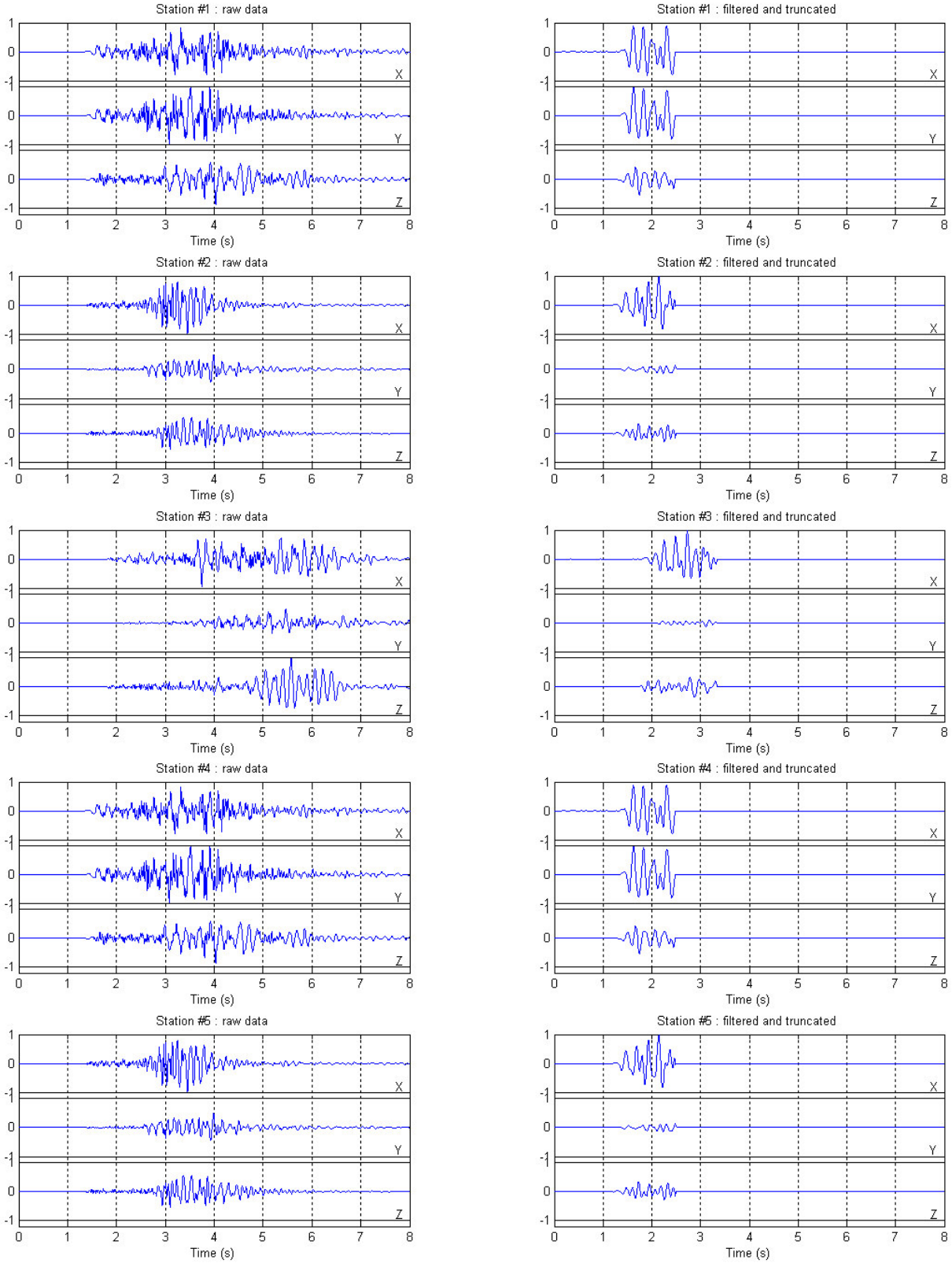

Figure 21. Three component records
Left: raw data; Right: data after applying a filter and a time window

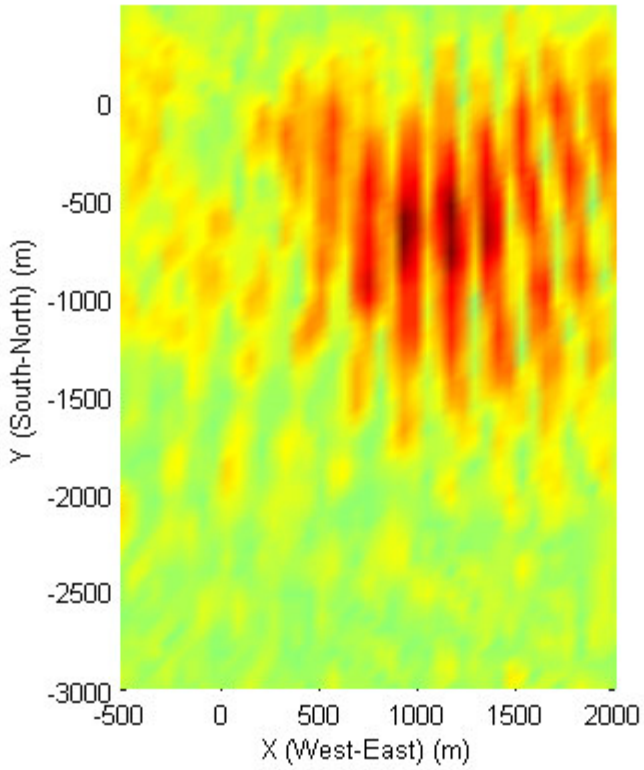

Figure 22. Snapshot result, X-Y slice at one possible depth.